JOURNAL OF GUIDANCE, CONTROL, AND DYNAMICS
Vol. 22, No. 2, March–April 1999

Asymmetric Body Spinning Motion with Energy Dissipation and Constant Body-Fixed Torques

Rafael Livneh* and Bong Wie†
Arizona State University, Tempe, Arizona 85287-6106

The spinning motion of an asymmetric body under the influence of both energy dissipation and constant body-fixed torques is investigated using a generic semirigid model with a spherical slug surrounded by a viscous layer. The study objective was to achieve a more fundamental understanding of the general spinning motion of a semirigid spacecraft during a typical spin-up maneuver, a flat-spin transition maneuver, and/or a flat-spin recovery maneuver. A set of nondimensional equations of motion is derived for the stability analysis of equilibrium points. In particular, three-dimensional phase-space trajectories are studied for three different cases of constant body-fixed torques along the major, intermediate, or minor axis. For these cases with energy dissipation, some new analytical as well as computer simulation results are discussed in terms of equilibrium manifolds, separatrix surfaces, periodic or nonperiodic solutions, etc.

Introduction

FOR a torque-free semirigid body with internal energy dissipation, the kinetic energy decreases and the energy ellipsoid becomes smaller with time. This results in an open polhode path that spirals outward from the minor axis, crosses the separatrix, and approaches the major axis. Consequently, a spacecraft spinning about its minor axis in the presence of energy dissipation is said to be unstable; i.e., the spacecraft will eventually reorient and spin about its major axis with either a positive or negative spin rate. A classic example of the minor-axis instability phenomenon is the first U.S. satellite, Explorer I, launched in 1958.

Although a spacecraft spinning about its minor axis is unstable in the presence of internal energy dissipation, spacecraft are often required to spin about their minor axis for several reasons. Fairing constraints of most launch vehicles require that the minor axis of the payload spacecraft be aligned with the longitudinal axis of the launch vehicles. Furthermore, most launch vehicles spin about their longitudinal axis before payload separation, resulting in a minor-axis spin of the spacecraft after separation.

Some launch vehicles or upper stages do not have spin-up capability for payload spacecraft and spin-up of the spacecraft is achieved after separation. Because of initial angular rates at separation, a typical spin-up maneuver usually results in a residual nutation angle and a spin-axis precession from the separation attitude. The spin rate selection depends on many factors, including the pointing accuracy requirement.

Spacecraft spinning about their minor axis are often stabilized using an active nutation control system consisting of thrusters and accelerometers. Spinning spacecraft are also required to spin down or reorient their spin axis during the various phases of spacecraft operation. For example, a spin-axis reorientation is required to align the spacecraft spin axis in the proper direction for apogee-kick motor firing. After apogee-kick motor burn, a spin-axis reorientation is also required to orient the spin axis to the orbit normal. During the operational life of spin-stabilized spacecraft, periodic spin-axis reorientation maneuvers are also required to compensate for the effects of external disturbance torques, primarily caused by solar pressures.

One of the simplest rotational maneuvers is the reorientation of the spin axis of a spacecraft using internal energy dissipation. A semirigid spacecraft with internal energy dissipation is stable only when spinning about its major axis. A spacecraft spinning about its minor axis in the presence of energy dissipation is unstable; i.e., the spacecraft will eventually reorient to spin about its major axis. Such a passive reorientation maneuver is called a flat-spin transition maneuver. The orientation of the spacecraft relative to the inertially fixed angular momentum vector at the end of the maneuver is, however, unpredictable; i.e., the spacecraft can end up with either a positive or a negative spin about the major axis.

To study such a flat-spin transition maneuver, Rahn and Barba[1] considered a rigid body with a spherical fuel slug that is surrounded by a viscous fluid layer. The passive, flat-spin transition maneuver, when augmented by few thruster firings based on rate gyro signals, can provide a predetermined, final spin polarity, however. For example, a control logic proposed by Rahn and Barba[1] utilizes angular rate sign changes to determine when a separatrix has been crossed and when thrusters must be fired. The sizing of the thruster firings is, however, based on estimates of the energy dissipation in the spacecraft.

A transition from a spinning mode to a bias-momentum stabilized mode of a three-axis stabilized spacecraft is often achieved by applying a constant torque to a wheel that is initially orthogonal to the spacecraft momentum vector, thus causing angular momentum transfer from the spinning spacecraft to the wheel. Such an attitude acquisition maneuver scheme, developed in Barba and Aubrun,[2] simultaneously achieves final despin of a spinning spacecraft, wheel spin-up, and a proper reorientation of the spacecraft. A similar procedure is also applicable to the recovery of dual-spin-stabilized or spinning spacecraft, which is known as the flat-spin recovery maneuver.[3]

In this paper we will study a generic model of a spinning, asymmetric spacecraft under the influence of both energy dissipation and constant body-fixed torques. The purpose is to provide a more fundamental understanding of the spinning motion of a semirigid spacecraft during various rotational maneuvers, such as a typical spin-up maneuver, a flat-spin transition maneuver with spin polarity control, or a flat-spin recovery maneuver using spin-up thrusters.

The main results of this paper can be summarized as follows: 1) for constant torque about the major axis, we have a typical major-axis, spin-up maneuver; 2) for torque about either the minor or intermediate axis, the spacecraft approaches an equilibrium point with a large angular velocity component about the major axis; 3) the polarity of the final equilibrium point is sensitive to initial conditions and also tends to converge to the nearest branch of the corresponding hyperbola of equilibrium points; and 4) for a certain case with a constant minor-axis torque, the spacecraft continues to spin about the minor axis before converging to an equilibrium point with a large angular velocity component along the major axis.

Received May 9, 1997; revision received Aug. 2, 1998; accepted for publication Sept. 3, 1998.

*Research Scientist, Aerospace Research Center; currently Member of the Technical Staff, Flight Control Systems, Boeing Company, 5000 E. McDowell Road, Mesa, AZ 85215. Senior Member AIAA.

†Professor, Department of Mechanical and Aerospace Engineering. Associate Fellow AIAA.

Similar to the case of a general rigid body under the influence of constant body-fixed torques, described in Refs. 4 and 5, we first derive a set of nondimensional equations of motion of a semirigid body subject to constant body-fixed torques for the stability analysis of its equilibrium points.

Equations of Motion

The effect of energy dissipation on the rotational motion of a spacecraft subject to constant body-fixed torques can be investigated simply by considering a spacecraft model with a spherical slug of inertia J, which is centered about the center of mass of the spacecraft and surrounded by a viscous layer of viscosity δ. The rotational equations of motion of such a simple semirigid spacecraft are given by[1]

$$(I_1 - J)\dot{\omega}_1 - (I_2 - I_3)\omega_2\omega_3 - \delta\sigma_1 = M_1 \tag{1}$$

$$(I_2 - J)\dot{\omega}_2 - (I_3 - I_1)\omega_1\omega_3 - \delta\sigma_2 = M_2 \tag{2}$$

$$(I_3 - J)\dot{\omega}_3 - (I_1 - I_2)\omega_1\omega_2 - \delta\sigma_3 = M_3 \tag{3}$$

$$\dot{\sigma}_1 + \dot{\omega}_1 + (\delta/J)\sigma_1 + \omega_2\sigma_3 - \omega_3\sigma_2 = 0 \tag{4}$$

$$\dot{\sigma}_2 + \dot{\omega}_2 + (\delta/J)\sigma_2 + \omega_3\sigma_1 - \omega_1\sigma_3 = 0 \tag{5}$$

$$\dot{\sigma}_3 + \dot{\omega}_3 + (\delta/J)\sigma_3 + \omega_1\sigma_2 - \omega_2\sigma_1 = 0 \tag{6}$$

where I_1, I_2, and I_3 are the principal moments of inertia of the main body plus the spherical slug of inertia J; ω_1, ω_2, and ω_3 are the angular velocity vector components of the main body; M_1, M_2, and M_3 are the constant body-fixed torque vector components; σ_1, σ_2, and σ_3 are the angular velocity vector components of the spherical slug relative to the main body; and the overdot denotes the differentiation with respect to time t.

Let

$$\alpha_i \equiv \frac{I_i - J}{J}, \qquad u_i \equiv \frac{M_i}{I_i - J}, \qquad k_1 \equiv \frac{\alpha_2 - \alpha_3}{\alpha_1}$$

$$k_2 \equiv \frac{\alpha_1 - \alpha_3}{\alpha_2}, \qquad k_3 \equiv \frac{\alpha_1 - \alpha_2}{\alpha_3}, \qquad k \equiv k_1k_2k_3$$

$$\tau \equiv t\sqrt{k}, \qquad \zeta \equiv \frac{\delta}{J\sqrt{k}}, \qquad \mu_i \equiv \frac{1}{\sqrt{k}}\left(\frac{u_i}{k_i}\right) \tag{7}$$

$$x_i \equiv \frac{\omega_i}{\sqrt{k_i}}, \qquad y_i \equiv \frac{\sigma_i}{\sqrt{k_i}}, \qquad i = 1, 2, 3$$

where the various α_i are the nondimensional inertia parameters, and τ, ζ, x_i, y_i, and μ_i are the scaled quantities associated with the time, damping, spacecraft angular velocity, angular velocity of the spherical slug, and the time-varying body-fixed torque, respectively. Then we can rewrite Eqs. (1–6) as

$$\frac{dx_1}{d\tau} - x_2x_3 - \frac{\zeta}{\alpha_1}y_1 = \mu_1 \tag{8}$$

$$\frac{dx_2}{d\tau} + x_1x_3 - \frac{\zeta}{\alpha_2}y_2 = \mu_2 \tag{9}$$

$$\frac{dx_3}{d\tau} - x_1x_2 - \frac{\zeta}{\alpha_3}y_3 = \mu_3 \tag{10}$$

$$\frac{dy_1}{d\tau} + \frac{dx_1}{d\tau} + \zeta y_1 + \frac{1}{k_1}(x_2y_3 - x_3y_2) = 0 \tag{11}$$

$$\frac{dy_2}{d\tau} + \frac{dx_2}{d\tau} + \zeta y_2 + \frac{1}{k_2}(x_3y_1 - x_1y_3) = 0 \tag{12}$$

$$\frac{dy_3}{d\tau} + \frac{dx_3}{d\tau} + \zeta y_3 + \frac{1}{k_3}(x_1y_2 - x_2y_1) = 0 \tag{13}$$

For the special case of a constant body-fixed torque vector, we can further eliminate the dependence of Eqs. (1–3) on the magnitude of the torque vectors M_1, M_2, and M_3 as follows. Let

$$u \equiv \frac{\sqrt{k_2k_3u_1^2 + k_1k_3u_2^2 + k_1k_2u_3^2}}{k} \tag{14}$$

and also define τ, ζ, μ_i, x_i, and y_i as

$$\tau = t\sqrt{ku}, \qquad \zeta \equiv \delta \Big/ J\sqrt{ku}, \qquad \mu_i \equiv \left(1 \Big/ u\sqrt{k}\right)\left(u_i \Big/ \sqrt{k_i}\right)$$

$$x_i \equiv \omega_i \Big/ \sqrt{uk_i}, \qquad y_i \equiv \sigma_i \Big/ \sqrt{k_iu}$$

$$i = 1, 2, 3 \tag{15}$$

Then, we can rewrite Eqs. (1–6) as Eqs. (8–13) with the following constraint:

$$\mu_1^2 + \mu_2^2 + \mu_3^2 = 1 \tag{16}$$

Because k_1, k_2, and k_3 are defined in terms of α_1, α_2, and α_3, the nondimensional formulation of the rotational dynamics of a damped semirigid body of Eqs. (8–13) depends only on four independent parameters, namely, α_1, α_2, α_3, and ζ, compared with the case of the dimensional formulation of Eqs. (1–6) with the five parameters I_1, I_2, I_3, J, and δ. Contrary to the complete independence of the nondimensional formulation for the rigid system on its inertial properties,[4] the nondimensional formulation of Eqs. (8–13) for the semirigid body is dependent upon the system's inertial and damping characteristics.

The equations of motion at steady state become

$$-X_2X_3 - (\zeta/\alpha_1)Y_1 = \mu_1 \tag{17}$$

$$X_1X_3 - (\zeta/\alpha_2)Y_2 = \mu_2 \tag{18}$$

$$-X_1X_2 - (\zeta/\alpha_3)Y_3 = \mu_3 \tag{19}$$

$$X_2Y_3 - X_3Y_2 + k_1\zeta Y_1 = 0 \tag{20}$$

$$X_3Y_1 - X_1Y_3 + k_2\zeta Y_2 = 0 \tag{21}$$

$$X_1Y_2 - X_2Y_1 + k_3\zeta Y_3 = 0 \tag{22}$$

where $(X_1, X_2, X_3, Y_1, Y_2, Y_3)$ denotes the equilibrium point. For a semirigid spacecraft, combining Eqs. (17–22) gives

$$k_1Y_1^2 + k_2Y_2^2 + k_3Y_3^2 = 0 \tag{23}$$

which can be satisfied if and only if

$$Y_1 = Y_2 = Y_3 = 0 \tag{24}$$

Substituting Eq. (24) into Eqs. (17–22) yields

$$(\mu_1, \mu_2, \mu_3) = (-X_2X_3, X_1X_3, -X_1X_2) \tag{25}$$

Hence we can readily conclude that both the damped and the undamped cases have the same equilibrium points for the angular velocities with the additional condition of equilibrium points at zero for $(\sigma_1, \sigma_2, \sigma_3)$ in the damped case. Defining the state perturbation terms as

$$\Delta x_i \equiv x_i - X_i, \qquad \Delta y_i \equiv y_i - Y_i, \qquad i = 1, 2, 3 \tag{26}$$

and keeping μ_i constant, we obtain the linearized equations of motion about the equilibrium point as

$$\begin{pmatrix} \Delta\dot{x}_1 \\ \Delta\dot{x}_2 \\ \Delta\dot{x}_3 \\ \Delta\dot{y}_1 \\ \Delta\dot{y}_2 \\ \Delta\dot{y}_3 \end{pmatrix} = \begin{pmatrix} 0 & X_3 & X_2 & s_1\zeta & 0 & 0 \\ -X_3 & 0 & -X_1 & 0 & s_2\zeta & 0 \\ X_2 & X_1 & 0 & 0 & 0 & s_3\zeta \\ 0 & -X_3 & -X_2 & -(s_1+1)\zeta & r_1X_3 & -r_1X_2 \\ X_3 & 0 & X_1 & -r_2X_3 & -(s_2+1)\zeta & r_2X_1 \\ -X_2 & -X_1 & 0 & r_3X_2 & -r_3X_1 & -(s_3+1)\zeta \end{pmatrix} \begin{pmatrix} \Delta x_1 \\ \Delta x_2 \\ \Delta x_3 \\ \Delta y_1 \\ \Delta y_2 \\ \Delta y_3 \end{pmatrix} \tag{27}$$

where $r_i = 1/k_i$ and $s_i = 1/\alpha_i$, $i = 1, 2, 3$.

Defining

$$b_1 \equiv s_1 + s_2 + s_3, \qquad b_2 \equiv X_1^2 - X_2^2 + X_3^2$$

$$b_3 \equiv r_2r_3X_1^2 - r_1r_3X_2^2 + r_1r_2X_3^2, \qquad b_4 \equiv s_1s_2 + s_1s_3 + s_2s_3$$

$$b_5 \equiv s_1X_1^2 - s_2X_2^2 + s_3X_3^2$$

$$b_6 \equiv r_3s_3\left(X_1^2 + X_2^2\right) + r_2s_2\left(X_1^2 - X_3^2\right) - r_1s_1\left(X_2^2 + X_3^2\right)$$

$$b_7 \equiv r_2r_3s_1X_1^2 + r_1r_3s_2X_2^2 + r_1r_2X_3^2$$

$$\begin{aligned} b_8 \equiv{}& s_1\left(r_2r_3X_1^2 - r_1r_3X_2^2 - r_1r_2X_3^2\right)X_1^2 \\ &+ s_2\left(r_2r_3X_1^2 - r_1r_3X_2^2 + r_1r_2X_3^2\right)X_2^2 \\ &+ s_3\left(-r_2r_3X_1^2 - r_1r_3X_2^2 + r_1r_2X_3^2\right)X_3^2 \end{aligned} \tag{28}$$

$$b_9 \equiv (r_2s_2 + r_3s_3)s_1X_1^2 - (r_1s_1 - r_3s_3)s_2X_2^2 - (r_1s_1 + r_2s_2)s_3X_3^2$$

$$b_{10} \equiv (r_2 - r_3)r_1s_1 + (r_1 + r_3)r_2s_2 - (r_1 - r_2)r_3s_3$$

$$b_{11} \equiv X_1X_2X_3$$

we obtain the characteristic equation as

$$\lambda^6 + a_1\lambda^5 + a_2\lambda^4 + a_3\lambda^3 + a_4\lambda^2 + a_5\lambda + a_6 = 0 \tag{29}$$

where

$$a_1 = (b_1 + 3), \qquad a_2 = (2b_1 + b_4 + 3)\zeta^2 + b_2 + b_3$$

$$\begin{aligned} a_3 ={}& (b_1 + b_4 + s_1s_2s_3 + 1)\zeta^3 \\ &+ (3b_2 + b_3 + b_5 + b_6 + b_7)\zeta + 2b_{11} \\ a_4 ={}& (3b_2 + 2b_5 + b_6 + b_9)\zeta^2 + (b_{10} + 6)b_{11}\zeta + b_2b_3 \\ a_5 ={}& (b_2 + b_5)\zeta^3 + 6b_{11}\zeta^2 + (b_2b_3 + b_8)\zeta + 2b_3b_{11} \\ a_6 ={}& 2b_{11}\left(b_3 + \zeta^2\right)\zeta \end{aligned} \tag{30}$$

From Eq. (25) we notice that $|\mu_1| = 1 \Rightarrow X_1 = 0$, $|\mu_2| = 1 \Rightarrow X_2 = 0$, and $|\mu_3| = 1 \Rightarrow X_3 = 0$. For these cases, $b_{11} = 0$ results in $a_6 = 0$, which means that the linearized system has a zero eigenvalue about the corresponding hyperbolas of equilibrium points. A numerical stability test seems to be the most viable option to determine the stability of the remaining five eigenvalues of the linearized system about these equilibria. As in the undamped case, for a general constant torque case (i.e., $\mu_1\mu_2 \neq 0$, $\mu_1\mu_3 \neq 0$, or $\mu_2\mu_3 \neq 0$), the damped system has no equilibrium points.

Simulation Results

Typical phase-space trajectories of a semirigid spacecraft subjected to a constant body-fixed torque about either its major, minor, or intermediate axis are shown in Figs. 1–9. For detailed discussion of the terminology used to describe the results, such as separatrix surfaces and stable/unstable regions, see Ref. 4 or 5. All numerical simulations were performed for the case of $(I_1, I_2, I_3) = (2000, 1500, 1000)$ kg·m^2, studied by Rahn and Barba.[1]

Major-Axis Torque

Figures 1–3 correspond to a case of constant torque about the major axis with $J = 100$ kg·m^2, $\delta = 45.52$ N·m·s, and $(M_1, M_2, M_3) = (25, 0, 0)$ N·m, for three different initial conditions. In Fig. 1, the trajectory starts from the lower unstable region of the (x_1, x_2, x_3) space. The top figure shown in Fig. 1 depicts the two-dimensional projections of the trajectory on the (x_1, x_2), (x_1, x_3), and (x_2, x_3) planes superimposed on three-dimensional separatrix surfaces. Also shown in Fig. 1 are the (x_1, x_3) projections of both the

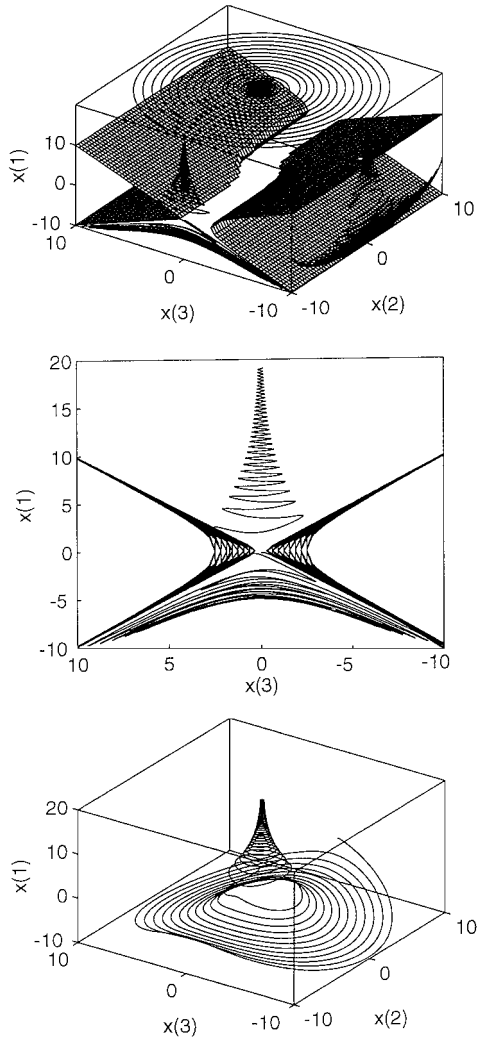

Fig. 1 Typical trajectories for major-axis torque with α = (19, 14, 9), ζ = 5, μ = (1, 0, 0), $x(0)$ = (−0.2, 10, 0), and τ_f = 35.

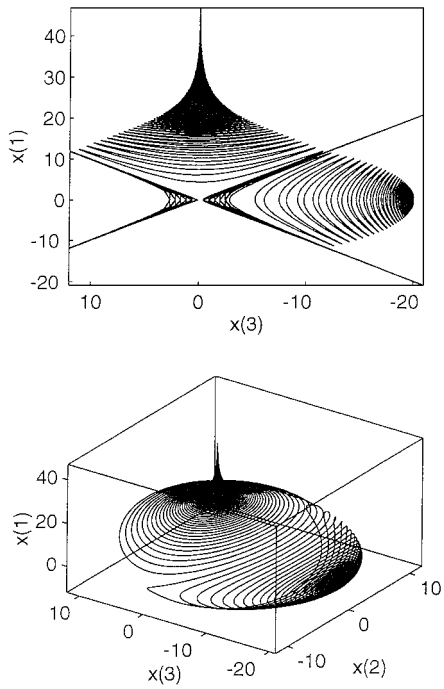

Fig. 2 Typical trajectories for major-axis torque with $\alpha = (19, 14, 9)$, $\zeta = 5$, $\mu = (1, 0, 0)$, $x(0) = (0, 1, -20)$, and $\tau_f = 50$.

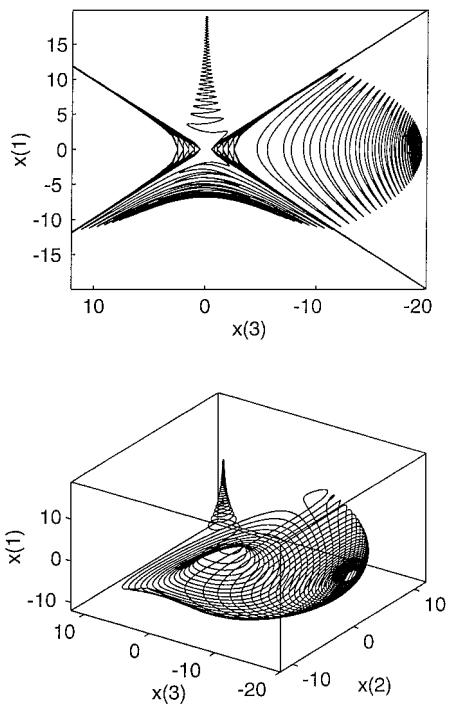

Fig. 3 Typical trajectories for major-axis torque with $\alpha = (19, 14, 9)$, $\zeta = 5$, $\mu = (1, 0, 0)$, $x(0) = (0, 1, -19.5)$, and $\tau_f = 50$.

trajectory and the two separatrix surfaces and a three-dimensional view of the trajectory without the separatrix surfaces. (Figures 2–9 follow similar graphical formats.) It is interesting to note that the trajectory in Fig. 1 does not cross the rigid-body separatrix surfaces.[4,5] Rather, it progresses first down and then up to the upper unstable region, where it converges to a pure spin-up maneuver about x_1, with no angular velocity components about either x_2 or x_3.

Simulation results with the initial condition $\boldsymbol{x}(0) = (0, 1, -20)$ inside the negative x_3 stable region are shown in Fig. 2. The trajectory moves toward the separatrix surface with increased oscillatory amplitude. It then crosses into the positive unstable region, where it converges to a pure spin-up maneuver about x_1, with no angular velocity components about either x_2 or x_3.

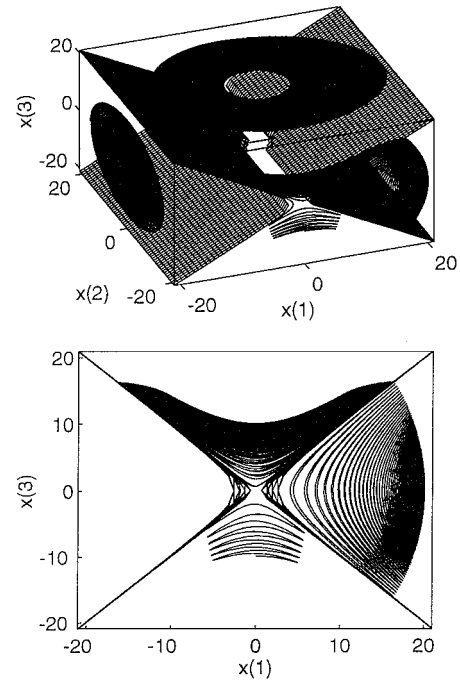

Fig. 4 Typical trajectories for minor-axis torque with $\alpha = (99, 74, 49)$, $\zeta = 14.6$, $\mu = (0, 0, 1)$, $x(0) = (0, -5, -9.9)$, and $\tau_f = 100$.

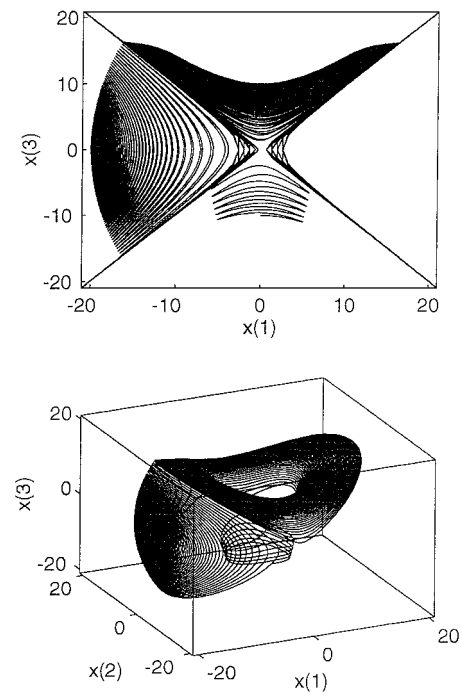

Fig. 5 Typical trajectories for minor-axis torque with $\alpha = (99, 74, 49)$, $\zeta = 14.6$, $\mu = (0, 0, 1)$, $x(0) = (0, -5, -10)$, and $\tau_f = 100$.

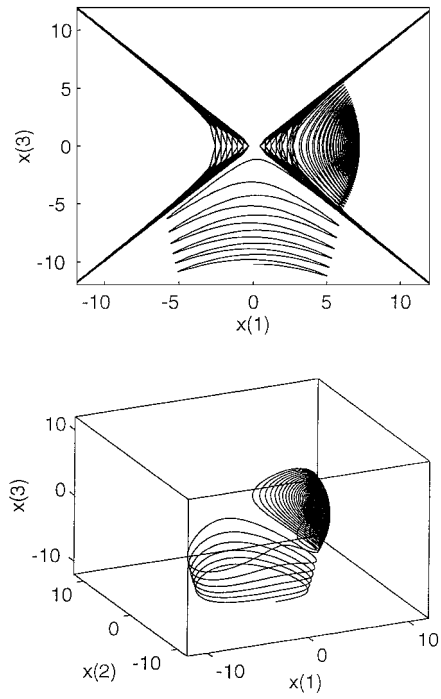

Fig. 6 Typical trajectories for minor-axis torque with $\alpha = (99, 74, 49)$, $\zeta = 14.6$, $\mu = (0, 0, 1)$, $x(0) = (0, -5, -10.2)$, and $\tau_f = 100$.

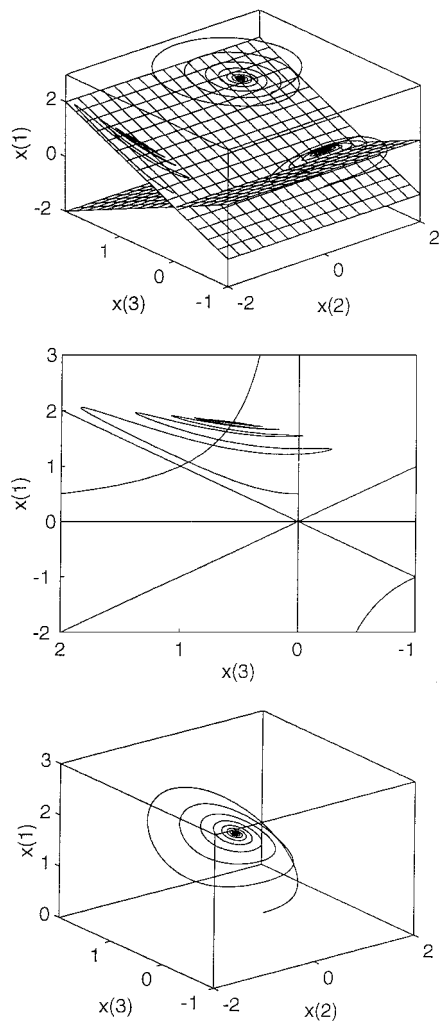

Fig. 7 Typical trajectories for intermediate-axis torque with $\alpha = (9, 6.5, 4)$, $\zeta = 1.675$, $\mu = (0, 1, 0)$, $x(0) = (0.5, 0, 0)$, and $\tau_f = 50$.

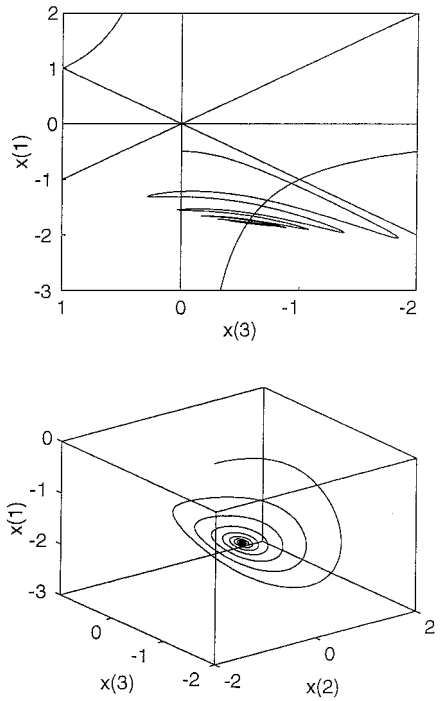

Fig. 8 Typical trajectories for intermediate-axis torque with $\alpha = (9, 6.5, 4)$, $\zeta = 1.675$, $\mu = (0, 1, 0)$, $x(0) = (-0.5, 0, 0)$, and $\tau_f = 50$.

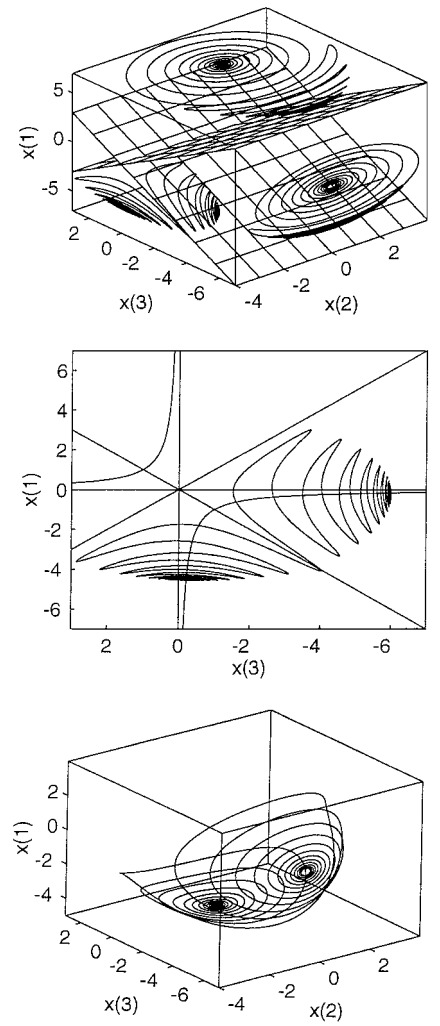

Fig. 9 Typical trajectories for intermediate-axis torque with $\alpha = (9, 6.5, 4)$, $\zeta = 2.65$, $\mu = (0, 1, 0)$, $x(0) = (0, 0, -6)$, and $\tau_f = 50$.

The result of a small perturbation in the initial conditions of Fig. 2 as $\boldsymbol{x}(0) = (0, 1, -19.5)$ is shown in Fig. 3. As can be seen, the resulting trajectory moves toward the separatrix surface with an increased oscillatory amplitude. It then crosses the separatrix surface into the lower part of the unstable region, where it reproduces the characteristics of the spinning motion shown in Fig. 1; i.e., it progresses first down and then up to the upper unstable region, where it converges to a pure spin-up maneuver about x_1.

Minor-Axis Torque

Figures 4–6 correspond to a case of constant torque about the minor axis with $J = 20\ \text{kg}\cdot\text{m}^2$, $\delta = 30\ \text{N}\cdot\text{m}\cdot\text{s}$, and $(M_1, M_2, M_3) = (0, 0, 25)\ \text{N}\cdot\text{m}$ for three different initial conditions.

In Fig. 4 the trajectory starts from $\boldsymbol{x}(0) = (0, -5, -9.9)$ at the lower unstable region, and it spins through the opening between the two separatrix surfaces and into the upper part of the unstable region, where a temporary spin-up in x_3 and also moderate increases in the amplitude of x_1 and x_2 are encountered. These changes are terminated by a flare-up in the magnitude of x_1 and x_2 that coincides with a decrease in the magnitude of the spin in x_3. This behavior is somewhat unexpected in the sense that a positive minor-axis torque ($M_3 > 0$) results in a despin about x_3. The combined effect of $M_3 > 0$ and the damping is to extract energy from the x_3 component of the rotation and to transfer the energy into x_1 and x_2. The increase in x_1 and x_2 eventually results in crossing the right separatrix and a temporary spin-up in x_1. Clearly, the combined effect of $M_3 > 0$ and the damping in the stable region is to extract energy from the x_2 and x_3 components and to transfer the energy to the major axis. The motion approaches a steady-state equilibrium rotation about $x_1 \cong 18$ and $x_2 \cong -1/18$, whereas x_3, σ_1, σ_2, and σ_3 all converge to zero as expected. A constant minor-axis torque $M_3 > 0$, which should have yielded a spin-up maneuver about the minor axis x_3 for an undamped system, results in a steady spin motion mainly about the positive x_1 value with a small component $x_2 \cong -1/x_1$.

Figure 5 shows the results of a small perturbation of -1% in the initial condition in x_3. As can be seen in Fig. 5, the motion starts with a spin-up to a positive value of x_3. This leads to a flare-up in the magnitude of x_1 and x_2, which coincides with a decrease in the magnitude of x_3. The main difference between the two cases is that the decrease in the magnitude of the spin in x_3 results in crossing the left separatrix to a local spin-up in $-x_1$ until reaching a steady state at $x_1 \cong -20$ and $x_2 \cong 1/20$.

A further 2% decrease in the value of the initial condition in x_3 leads to the spinning motion shown in Fig. 6. The angular velocity trajectory crosses the right separatrix into the right stable region (without passing through the upper unstable region), where it encounters an increase in x_1 until reaching a steady state at $x_1 \cong 7$ and $x_2 \cong -1/7$.

Similar to the torque-free, semirigid spacecraft case studied by Rahn and Barba,[1] a semirigid spacecraft subjected to a constant torque about its minor axis may also end up with either a positive or a negative major-axis spin. The differences between the torque-free and the minor-axis, constant-torque case are as follows: 1) angular momentum is not conserved; 2) the motion converges to an equilibrium point on the section of the hyperbola $X_1 X_2 = -1$, contained in region $|x_1| > |x_2|$; and 3) the sensitivity of the trajectory to initial conditions is manifested not only in the final sign of the spin about the major axis but also in the characteristics of the trajectory leading to the major-axis spin because the spacecraft can reach the two possible major-axis spin directions following a total of four qualitatively different trajectories.

Intermediate-Axis Torque

Figures 7–10 correspond to a case of constant torque about the intermediate axis with $J = 200\ \text{kg}\cdot\text{m}^2$, $\delta = 30\ \text{N}\cdot\text{m}\cdot\text{s}$, and $(M_1, M_2, M_3) = (0, 25, 0)\ \text{N}\cdot\text{m}$ for three different initial conditions.

In Fig. 7 the spinning motion starts from the region of $x_1 > |x_3|$. This motion remains confined to that region and rapidly converges to $x_1 \cong 1.8$ and $x_3 \cong 1/1.8 = 0.555$, whereas x_2, σ_1, σ_2, and σ_3 all converge to zero as expected.

Spinning motion initiated from the region of $-x_1 > |x_3|$ is shown in Fig. 8. This motion remains confined to that region and rapidly converges to $x_1 \cong -1.8$ and $x_3 \cong -1/1.8 = -0.555$, whereas x_2, σ_1, σ_2, and σ_3 all converge to zero.

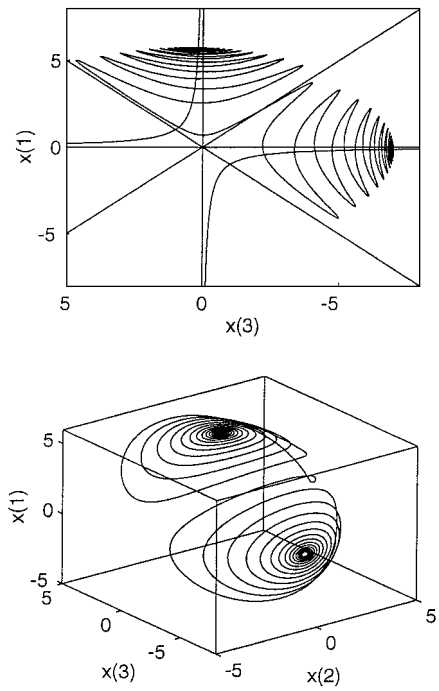

Fig. 10 Typical trajectories for intermediate-axis torque with α = (9, 6.5, 4), ζ = 2.65, μ = (0, 1, 0), x (0) = (0, 0, − 7), and τ_f = 50.

In Fig. 9 the spinning motion is initiated from the region of $x_3 < -|x_1|$. The trajectory moves toward the separatrix surface with increased oscillatory amplitude about the branch of the hyperbola $x_1 x_3 = 1$ contained in the region of $x_3 < -|x_1|$. It then crosses the lower left separatrix plane into the region of $-x_1 > |x_3|$, where it oscillates with decreasing amplitude about $x_1 x_3 = 1$ and rapidly converges to $x_1 \cong -4.6$ and $x_3 \cong -1/4.6 = -0.217$, whereas x_2, σ_1, σ_2, and σ_3 all converge to zero.

Similar to the case of minor-axis torque ($M_3 > 0$), shown in Figs. 4–6, the spacecraft may end up with either a positive or a negative major-axis spin rate. This fact is demonstrated in Fig. 10, in which changing the initial conditions from $\boldsymbol{x}(0) = (0, 0, -6)$ to $\boldsymbol{x}(0) = (0, 0, -7)$ resulted in an upper right separatrix crossing followed by oscillation about the positive branch of $x_1 x_3 = 1$ contained in the $x_3 > |x_1|$ region and rapid convergence to $x_1 \cong 5.8$ and $x_3 \cong 1/5.8 = 0.172$. An interesting observation regarding the case of intermediate-axis torque ($M_2 > 0$) is that a trajectory started from $\boldsymbol{x}(0) = (0, 0, -p)$, where $p > 0$, will tend to converge to the negative branch of $X_1 X_3 = 1$. This tendency decreases, however, as p increases. In the case of $(\alpha_1, \alpha_2, \alpha_3) = (9, 6.5, 4)$ and $\zeta = 2.65$, shown in Figs. 9 and 10, for example, the values of $p = 1, 2, 3, \ldots, 6$ all resulted in a final spin with negative major-axis spin rate.

All cases simulated for a constant intermediate-axis torque ended up converging to an equilibrium point on the section of the hyperbola $X_1 X_3 = 1$, contained in the region of $|x_1| > |x_3|$. Trajectories with initial conditions satisfying $|x_1(0)| < |x_3(0)|$ ended up crossing the separatrix surface once, whereas trajectories with initial conditions satisfying $|x_1(0)| > |x_3(0)|$ did not cross the separatrix surface.

Note that all of the cases presented in this paper correspond only to a constant torque about a principal-axis direction. Preliminary analysis suggests the existence of stable equilibrium points for some cases of constant torque with components along all three principal-axis directions. The general stability analysis of Eq. (27) depends on the four independent parameters α_1, α_2, α_3, and ζ of the nondimensional formulation of Eqs. (8–13). Because of its anticipated complexity, this research topic is reserved for future work.

Conclusions

The spinning motion of a generic semirigid body with energy dissipation and constant body-fixed torque about one of its principal axes was investigated. The nondimensional equations of motion

were derived and shown to depend on four parameters only. The equilibrium condition of the semirigid body was shown to be identical to that of the rigid body with no relative motion between the fuel slug and the rigid body. The characteristic equation of the linearized system was analytically derived for numerical stability analysis. The main results of extensive simulations of a general semirigid body with constant torques about either its major, intermediate, or minor axis are as follows: 1) constant torque about the major axis resulted in a typical spin-up maneuver, as expected; 2) for torque about either the minor or the intermediate axis the spacecraft ended up rotating about an equilibrium point with a large angular velocity component along the major axis; 3) the polarity of the final equilibrium point is sensitive to initial conditions and also tends to converge to the nearest branch of the corresponding hyperbola of equilibrium points; and 4) for a certain case with a constant minor-axis torque, the spacecraft continued to spin about the minor axis before converging to an equilibrium point with a large angular velocity component along the major axis.

References

[1]Rahn, C. D., and Barba, P. M., "Reorientation Maneuver for Spinning Spacecraft," *Journal of Guidance, Control, and Dynamics*, Vol. 14, No. 4, 1991, pp. 724–728.

[2]Barba, P. M., and Aubrun, J. N., "Satellite Attitude Acquisition by Momentum Transfer," *AIAA Journal*, Vol. 14, No. 10, 1976, pp. 1382–1386.

[3]Barba, P. M., Furumoto, N., and Leliakov, I. P., "Techniques for Flat-Spin Recovery of Spinning Satellites," AIAA Paper 73-859, Key Biscayne, FL, Aug. 1973.

[4]Livneh, R., and Wie, B., "New Results for an Asymmetric Rigid Body with Constant Body-Fixed Torques," *Journal of Guidance, Control, and Dynamics*, Vol. 20, No. 5, 1997, pp. 873–881.

[5]Wie, B., *Space Vehicle Dynamics and Control*, AIAA Education Series, AIAA, Reston, VA, 1998, pp. 355–365.